 SDHM, vol.6, no.4, pp.329-350, 2010

Transient coupled thermoelastic crack analysis in functionally graded materials [1]

A.V. Ekhlakov[2], O.M. Khay[2], Ch. Zhang[2], J. Sladek[3] and V. Sladek[3]

Abstract: In this paper, transient crack analysis in two-dimensional, isotropic, continuously non-homogeneous and linear elastic functionally graded materials is presented. A boundary-domain element method based on boundary-domain integral representations is developed. The Laplace-transform technique is utilized to eliminate the dependence on time. Laplace-transformed fundamental solutions of linear coupled thermoelasticity for isotropic, homogeneous and linear elastic solids are applied to derive boundary-domain integral equations. The numerical implementation is performed by using a collocation method for the spatial discretization. The time-dependent numerical solutions are obtained by the Stehfest's inversion algorithm. For an edge crack in a finite domain under thermal shock, the dynamic stress intensity factors are presented and discussed.

Keywords: Functionally graded materials, Transient linear coupled thermoelasticity, Dynamic stress intensity factors, Boundary-domain element method, Laplace-transform technique

1 Introduction

Functionally graded materials (FGMs) represent a new generation of composites designed to achieve high-performance mechanical and thermal properties in comparison to the conventional composites and to gain the benefit from the properties of its constituents [Suresh and Mortensen (1998)]. FGMs are two-phase composite materials, for example, ceramic and metal alloys phases, in which the volume fractions of the constituents vary continuously in space. Therefore, those materials have a non-uniform microstructure with position dependent macro-properties and no interfaces. They possess the desirable properties of metals such as high toughness,

[1] In memory of Prof. Dr.-Ing. F.-G. Buchholz

[2] Department of Civil Engineering, University of Siegen, D-57068 Siegen, Germany

[3] Institute of Construction and Architecture, Slovak Academy of Sciences, 84503 Bratislava, Slovakia

high mechanical strength, bonding capability and high heat, wear and corrosion resistances of ceramics. FGMs can be employed to a wide range of engineering structures and components such as electronic devices, thermal and corrosion resistant coatings, blast protections as well as biomaterials [Paulino, Jin, and Dodds (2003)]. Because of the inherent brittle nature of ceramics cracks may develop in the manufacturing phase or during their services. Therefore, the crack analysis of FGMs under extreme thermal and mechanical loadings may provide a better understanding of the fracture properties, which are essential to their integrity, reliability and durability in practical engineering applications.

Initial-boundary value problems of transient linear coupled thermoelasticity for FGMs are described by the coupled partial differential equations with variable coefficients, to which analytical methods can be successfully applied only for very special simple geometry and loading conditions. In general cases, experimental and numerical methods have to be used for investigating crack problems in FGMs. In this context, we only mention some performed works for static problems [Jin and Noda (1994); Lee and Erdogan (1994); Erdogan and Wu (1996); Nemat-Alla and Noda (1996, 2000); Yildirim and Erdogan (2004); Ding and Li (2010)], for dynamic crack analysis under thermal shock [Erdogan and Rizk (1992); Noda, Ashida, and Matsunaga (1994); Jin and Paulino (2001); Jin (2004); Noda and Guo (2008); Guo and Noda (2010)] and for crack propagation problems under thermal shock [Fujimoto and Noda (2000, 2001); Noda, Ishihara, Yamamoto, and Fujimoto (2003); Batra and Love (2005)]. From the standpoint of numerical methods, the finite element method (FEM) [Anlas, Santare, and Lambros (2000); Santare and Lambros (2000); Lu, Liu, Jia, and Yu (2001); Kim and Paulino (2003, 2005); Yildirim (2006); Dag and Yildirim (2009); Zamani and Reza Eslami (2009)], the boundary element method (BEM) [Sládek, Sládek, and Markechova (1990, 1993); Balaš, Sládek, and Sládek (1989); Aliabadi (2002)] and the meshless local Petrov-Galerkin (MLPG) [Sládek, Sládek, and Zhang (2005); Sládek, Sládek, Zhang, and Tan (2006); Gao, Zhang, Sladek, and Sladek (2008); Sládek, Sládek, Solek, Tan, and Zhang (2009)] are often employed.

The BEM is a powerful, very accurate and efficient numerical method for fracture analysis. It has been successfully applied to coupled linear thermoelasticity in homogeneous solids [Dargush and Banerjee (1989, 1990, 1991); Tosaka and Suh (1991); Tanaka, Matsumoto, and Moradi (1995); Chen and Dargush (1995); Tehrani and Eslami (1998); Hosseini-Tehrani and Eslami (2000); Kögl and Gaul (2000, 2003)]. Katsareas and Anifantis (1995) have used a time-domain BEM to calculate stress intensity factors in the context of the quasi-static uncoupled theory of thermoleasticity. Hosseini-Tehrani, Eslami, and Daghyani (2001) and Hosseini-Tehrani and Hosseini-Godarzi (2004) have solved some dynamic crack problems

of coupled thermoelasticity by a Laplace-transformed BEM in a two-dimensional finite domain. Then, this BEM has been extended to the crack problems considering Lord-Shulman theory [Hosseini-Tehrani, Hosseini-Godarzi, and Tavangar (2005)]. A comparison of crack growth simulation by dual BEM (DBEM) and FEM for SEN-specimens undergoing torsion or bending loading has been presented by Citarella and Buchholz (2008). Unfortunately, BEM extensions and applications to FGMs are yet very limited, because the required fundamental solutions are either not available or mathematically too complex.

The focus of this paper is on the transient analysis of coupled thermoelastic crack problems in isotropic, continuously non-homogeneous and linear elastic FGMs under thermal shock by using a boundary-domain element method (BDEM). To eliminate the time-dependence in the governing equations the Laplace-transform technique is applied. Fundamental solutions for homogeneous and linear thermoelastic materials in Laplace-transformed domain are utilized to derive the boundary-domain integral equation representations for the mechanical and thermal fields. This approach leads to domain integrals involving the unknown quantities in addition to the conventional boundary integrals. The spatial discretization of the boundary-domain integral equations is performed by a collocation method. The arising boundary and domain integrals are computed after special regularization procedures [Aliabadi (2002)] by the standard Gaussian quadrature. To obtain time-dependent solutions an inverse Laplace-transform is performed by using the Stehfest's algorithm [Stehfest (1970)]. Numerical results are presented and discussed to show the influence of the material gradation and the thermo-mechanical coupling on the dynamic stress intensity factors (SIFs).

2 Boundary-domain integral equations

Let us consider a non-homogeneous, isotropic and linear elastic FGM in a two-dimensional (2-D) domain Ω. The material properties (mass density $\rho(\boldsymbol{x})$, Young's modulus $E(\boldsymbol{x})$, thermal conductivity $k(\boldsymbol{x})$, specific heat $c(\boldsymbol{x})$, linear thermal expansion coefficient $\alpha(\boldsymbol{x})$, etc) are assumed to be a differentiable function of spatial coordinates and the Poisson's ratio ν is taken as constant. In the absence of body forces and heat sources, the governing equations for the transient linear coupled thermoelasticity can be written as

$$\sigma_{ij,j}(\boldsymbol{x},t) - \rho(\boldsymbol{x})\,\ddot{u}_i(\boldsymbol{x},t) = 0, \tag{1}$$

$$\begin{aligned}\left[k(\boldsymbol{x})\,\theta_{,i}(\boldsymbol{x},t)\right]_{,i} &- \rho(\boldsymbol{x})c(\boldsymbol{x})\,\dot{\theta}(\boldsymbol{x},t) \\ &- \gamma(\boldsymbol{x})T_0\,\dot{u}_{k,k}(\boldsymbol{x},t) = 0,\end{aligned} \tag{2}$$

where σ_{ij}, u_i and θ are the stresses, displacements and temperature difference, respectively, $\gamma(\boldsymbol{x}) = E(\boldsymbol{x})\alpha(\boldsymbol{x})/(1-2\nu)$ is the stress-temperature modulus and T_0 is the reference temperature. Here, a comma after a quantity represents spatial derivatives, superscript dots indicate time derivatives and the summation convention for repeated indices is implied.

The relation between the stresses and the displacements with consideration of temperature changes is defined by the Duhamel-Neumann constitutive equations

$$\sigma_{ij}(\boldsymbol{x},t) = c_{ijkl}(\boldsymbol{x})u_{k,l}(\boldsymbol{x},t) - \gamma(\boldsymbol{x})\theta(\boldsymbol{x},t)\delta_{ij}, \tag{3}$$

where δ_{ij} is the Kronecker symbol. The elasticity tensor in Eq. (3) is given by

$$c_{ijkl}(\boldsymbol{x}) = \mu(\boldsymbol{x})\left[\frac{2\nu}{1-2\nu}\delta_{ij}\delta_{kl} + \delta_{ik}\delta_{jl} + \delta_{il}\delta_{jk}\right],$$

where $\mu(\boldsymbol{x}) = E(\boldsymbol{x})/2(1+\nu)$ is the shear modulus.

The boundary conditions for the mechanical and the thermal quantities are assumed to be as follows

$$\begin{aligned}
&u_i(\boldsymbol{x},t) = \tilde{u}_i(\boldsymbol{x},t) && \text{on} \quad \Gamma_u,\\
&t_i(\boldsymbol{x},t) = \sigma_{ij}(\boldsymbol{x},t)\,n_j(\boldsymbol{x}) = \tilde{t}_i(\boldsymbol{x},t) && \text{on} \quad \Gamma_t,\\
&\theta(\boldsymbol{x},t) = \tilde{\theta}(\boldsymbol{x},t) && \text{on} \quad \Gamma_\theta,\\
&q(\boldsymbol{x},t) = k(\boldsymbol{x})\theta_{,i}(\boldsymbol{x},t)\,n_j(\boldsymbol{x}) = \tilde{q}(\boldsymbol{x},t) && \text{on} \quad \Gamma_q,
\end{aligned} \tag{4}$$

where Γ_u and Γ_t are the parts of the boundary $\Gamma = \partial\Omega = \Gamma_u \cup \Gamma_t$, $\Gamma_u \cap \Gamma_t = \emptyset$, in which the displacements $\tilde{u}_i$ and the tractions $\tilde{t}_i$ are given; Γ_θ and Γ_q are the parts of the boundary $\Gamma = \Gamma_\theta \cup \Gamma_q$, $\Gamma_\theta \cap \Gamma_q = \emptyset$ with the specified temperature $\tilde{\theta}$ and heat flux $\tilde{q}$, respectively. The initial conditions are given by

$$\begin{aligned}
&u_i(\boldsymbol{x},t)|_{t=0} = \dot{u}_i(\boldsymbol{x},t)|_{t=0} = 0,\\
&\theta(\boldsymbol{x},t)|_{t=0} = 0.
\end{aligned} \tag{5}$$

Applying the Laplace-transform to the governing equations (1) and (2) yields

$$\begin{aligned}
&c_{ijkl}(\boldsymbol{x})\,\bar{u}_{k,lj}(\boldsymbol{x},p) - \gamma(\boldsymbol{x})\,\bar{\theta}_{,i}(\boldsymbol{x},p) - \rho(\boldsymbol{x})p^2\,\bar{u}_i(\boldsymbol{x},p)\\
&\qquad + c_{ijkl,j}(\boldsymbol{x})\,\bar{u}_{k,l}(\boldsymbol{x},p) - \gamma_{,i}(\boldsymbol{x})\,\bar{\theta}(\boldsymbol{x},p) = 0,
\end{aligned} \tag{6}$$

$$\begin{aligned}
&\bar{\theta}_{,ii}(\boldsymbol{x},p) - \beta^2(\boldsymbol{x})\,\bar{\theta}(\boldsymbol{x},p) - \eta(\boldsymbol{x})p\,\bar{u}_{k,k}(\boldsymbol{x},p)\\
&\qquad + \frac{k_{,i}(\boldsymbol{x})}{k(\boldsymbol{x})}\,\bar{\theta}_{,i}(\boldsymbol{x},p) = 0,
\end{aligned} \tag{7}$$

where p is the Laplace-transform parameter, $\kappa(\boldsymbol{x}) = k(\boldsymbol{x})/\rho(\boldsymbol{x})c(\boldsymbol{x})$ is the thermal diffusivity, $\eta(\boldsymbol{x}) = \gamma(\boldsymbol{x})T_0/k(\boldsymbol{x})$ and $\beta_0^2 = p/\kappa$, and the superimposed bar denotes the Laplace-transformed domain.

Integral representations of the displacements and the temperature at an arbitrary point $\boldsymbol{x} \in \Omega$ are derived from the generalized reciprocal theorem for FGMs by using the Laplace-transformed fundamental solutions of linear coupled thermoelasticity for homogeneous materials [Balaš, Sládek, and Sládek (1989)]

$$\begin{aligned}
\bar{u}_k(\boldsymbol{x},p) = &-\int_\Gamma [\bar{u}_i(\boldsymbol{y},p)\,\bar{T}_{ik}(\boldsymbol{x},\boldsymbol{y},p) \\
&-\frac{1}{\tilde{E}(\boldsymbol{y})\tilde{\alpha}(\boldsymbol{y})}\,\bar{t}_i(\boldsymbol{y},p)\,\bar{U}_{ik}(\boldsymbol{x},\boldsymbol{y},p)\Big]\,d\Gamma_y \\
&+\kappa_0\int_\Gamma \Big[\bar{\theta}(\boldsymbol{y},p)\,\bar{Z}_k(\boldsymbol{x},\boldsymbol{y},p) \\
&-\frac{\tilde{k}(\boldsymbol{y})}{\tilde{E}(\boldsymbol{y})\tilde{\alpha}(\boldsymbol{y})}\,\bar{q}(\boldsymbol{y},p)\,\bar{U}_k(\boldsymbol{x},\boldsymbol{y},p)\Big]\,d\Gamma_y + \bar{F}_k^{(u)}(\boldsymbol{x},p),
\end{aligned} \tag{8}$$

$$\begin{aligned}
\bar{\theta}(\boldsymbol{x},p) = &\frac{\kappa_0\eta_0 p}{\gamma_0}\int_\Gamma [\bar{u}_i(\boldsymbol{y},p)\,\bar{T}_i(\boldsymbol{x},\boldsymbol{y},p) \\
&-\frac{1}{\tilde{E}(\boldsymbol{y})\tilde{\alpha}(\boldsymbol{y})}\,\bar{t}_i(\boldsymbol{y},p)\,\bar{U}_i(\boldsymbol{x},\boldsymbol{y},p)\Big]\,d\Gamma_y \\
&-\kappa_0\int_\Gamma \Big[\bar{\theta}(\boldsymbol{y},p)\,\bar{F}(\boldsymbol{x},\boldsymbol{y},p) \\
&-\frac{\tilde{k}(\boldsymbol{y})}{\tilde{E}(\boldsymbol{y})\tilde{\alpha}(\boldsymbol{y})}\,\bar{\theta}(\boldsymbol{y},p)\,\bar{T}(\boldsymbol{x},\boldsymbol{y},p)\Big]\,d\Gamma_y + \bar{F}^{(\theta)}(\boldsymbol{x},p),
\end{aligned} \tag{9}$$

where $\boldsymbol{x}$ and $\boldsymbol{y}$ are the source and field points, respectively, a tilde over a quantity denotes the ratio of a non-homogeneous to a homogeneous quantity that is designated by a zero subscript. The functions $\bar{F}_k^{(u)}$ and $\bar{F}^{(\theta)}$ describe the material non-homogeneity and are defined in Appendix A. The functions $\bar{U}_{ij}(\boldsymbol{x},\boldsymbol{y},p)$, $\bar{U}_i(\boldsymbol{x},\boldsymbol{y},p)$, $\bar{T}(\boldsymbol{x},\boldsymbol{y},p)$ are the primary fields (displacements and temperature) and $\bar{T}_{ij}(\boldsymbol{x},\boldsymbol{y},p)$, $\bar{Z}_j(\boldsymbol{x},\boldsymbol{y},p)$, $\bar{F}(\boldsymbol{x},\boldsymbol{y},p)$ and $\bar{T}_i(\boldsymbol{x},\boldsymbol{y},p)$ are the secondary fields (tractions and heat flux) of the fundamental solutions of linear coupled thermoelasticity for a homogeneous solid in the Laplace-transformed domain [Balaš, Sládek, and Sládek (1989)]. It should be noted that Eqs. (8) and (9) are no longer pure boundary integral formulations because they involve domain integrals containing the unknown fields and their gradients.

By taking the limit $\boldsymbol{x} \to \Gamma$ and using the asymptotic behavior of the fundamental

solutions [Balaš, Sládek, and Sládek (1989)] the integral representations (8) and (9) are transformed into the boundary-domain integral equations (BDIEs)

$$
\begin{aligned}
&c_{ki}(\boldsymbol{x})\bar{u}_i(\boldsymbol{x},p)+\int_\Gamma [\bar{u}_i(\boldsymbol{y},p)\,\bar{T}_{ik}(\boldsymbol{x},\boldsymbol{y},p)\\
&-\frac{1}{\tilde{E}(\boldsymbol{y})\tilde{\alpha}(\boldsymbol{y})}\bar{t}_i(\boldsymbol{y},p)\,\bar{U}_{ik}(\boldsymbol{x},\boldsymbol{y},p)\Big]\,d\Gamma_y\\
&+\kappa_0\int_\Gamma\Big[\frac{\tilde{k}(\boldsymbol{y})}{\tilde{E}(\boldsymbol{y})\tilde{\alpha}(\boldsymbol{y})}\bar{q}(\boldsymbol{y},p)\,\bar{U}_k(\boldsymbol{x},\boldsymbol{y},p)\\
&-\bar{\theta}(\boldsymbol{y},p)\,\bar{Z}_k(\boldsymbol{x},\boldsymbol{y},p)\big]\,d\Gamma_y-\bar{F}_k^{(u)}(\boldsymbol{x},p)=0,
\end{aligned}
\tag{10}
$$

$$
\begin{aligned}
&c(\boldsymbol{x})\bar{\theta}(\boldsymbol{x},p)+\kappa_0\int_\Gamma\big[\bar{\theta}(\boldsymbol{y},p)\,\bar{F}(\boldsymbol{x},\boldsymbol{y},p)\\
&-\frac{\tilde{k}(\boldsymbol{y})}{\tilde{E}(\boldsymbol{y})\tilde{\alpha}(\boldsymbol{y})}\bar{q}(\boldsymbol{y},p)\,\bar{T}(\boldsymbol{x},\boldsymbol{y},p)\Big]\,d\Gamma_y\\
&+\frac{\kappa_0\eta_0 p}{\gamma_0}\int_\Gamma\Big[\frac{1}{\tilde{E}(\boldsymbol{y})\tilde{\alpha}(\boldsymbol{y})}\bar{t}_i(\boldsymbol{y},p)\,\bar{U}_i(\boldsymbol{x},\boldsymbol{y},p)\\
&-\bar{u}_i(\boldsymbol{y},p)\,\bar{T}_i(\boldsymbol{x},\boldsymbol{y},p)]\,d\Gamma_y-\bar{F}^{(\theta)}(\boldsymbol{x},p)=0.
\end{aligned}
\tag{11}
$$

The free-term coefficients $c_{ki}(\boldsymbol{x})$ and $c(\boldsymbol{x})$ depend on the shape of the boundary at the point $\boldsymbol{x}\in\Gamma$ and are expressed as

$$
\begin{aligned}
c_{ki}(\boldsymbol{x})&=-\int_\Gamma T_{ik}(\boldsymbol{x},\boldsymbol{y})\,d\Gamma_y,\\
c(\boldsymbol{x})&=-\kappa_0\int_\Gamma F(\boldsymbol{x},\boldsymbol{y})\,d\Gamma_y,
\end{aligned}
\tag{12}
$$

where $T_{ik}(\boldsymbol{x},\boldsymbol{y})$ and $F(\boldsymbol{x},\boldsymbol{y})$ are the static counterparts of the kernels $\bar{T}_{ik}(\boldsymbol{x},\boldsymbol{y},p)$ and $\bar{F}(\boldsymbol{x},\boldsymbol{y},p)$, respectively. It should be noted that the boundary and the domain integrals in the BDIEs (10) and (11) contain singular integrands. The strongly singular integrals in Eqs. (10) and (11) are understood as the Cauchy principal value integrals. The boundary integrals contain the strongly singular kernels $\bar{T}_{ij}(\boldsymbol{x},\boldsymbol{y},p)$ and $\bar{F}(\boldsymbol{x},\boldsymbol{y},p)$ as well as the weakly singular kernels $\bar{U}_{ij}(\boldsymbol{x},\boldsymbol{y},p)$, $\bar{Z}_i(\boldsymbol{x},\boldsymbol{y},p)$, $\bar{T}(\boldsymbol{x},\boldsymbol{y},p)$ and $\bar{T}_i(\boldsymbol{x},\boldsymbol{y},p)$. The domain integrals (see Eqs. (22) and (23) in Appendix A) at $\boldsymbol{x}\in\Gamma$ involve also the strongly singular kernels $\bar{T}_{,i}(\boldsymbol{x},\boldsymbol{y},p)$, $\bar{U}_{ij,k}(\boldsymbol{x},\boldsymbol{y},p)$ and the weakly singular kernel $\bar{U}_{i,j}(\boldsymbol{x},\boldsymbol{y},p)$. Making use of the singularity subtraction tech-

nique and using the notations (12) the BDIEs (10) and (11) are rewritten as

$$\begin{aligned}
&\bar{u}_i(\boldsymbol{x},p)\int_\Gamma [\bar{T}_{ik}(\boldsymbol{x},\boldsymbol{y},p)-T_{ik}(\boldsymbol{x},\boldsymbol{y})]\,d\Gamma_y\\
&+\int_\Gamma [\bar{u}_i(\boldsymbol{y},p)-\bar{u}_i(\boldsymbol{x},p)]\,\bar{T}_{ik}(\boldsymbol{x},\boldsymbol{y},p)\,d\Gamma_y\\
&-\int_\Gamma \frac{1}{\tilde{E}(\boldsymbol{y})\tilde{\alpha}(\boldsymbol{y})}\,\bar{t}_i(\boldsymbol{y},p)\bar{U}_{ik}(\boldsymbol{x},\boldsymbol{y},p)\,d\Gamma_y \qquad (13)\\
&+\kappa_0\int_\Gamma \left[\frac{\tilde{k}(\boldsymbol{y})}{\tilde{E}(\boldsymbol{y})\tilde{\alpha}(\boldsymbol{y})}\,\bar{q}(\boldsymbol{y},p)\,\bar{U}_k(\boldsymbol{x},\boldsymbol{y},p)\right.\\
&\left.-\bar{\theta}(\boldsymbol{y},p)\,\bar{Z}_k(\boldsymbol{x},\boldsymbol{y},p)\right]\,d\Gamma_y-\bar{F}_k^{(u)}(\boldsymbol{x},p)=0,\\
&\bar{\theta}(\boldsymbol{x},p)\kappa_0\int_\Gamma [\bar{F}(\boldsymbol{x},\boldsymbol{y},p)-F(\boldsymbol{x},\boldsymbol{y})]\,d\Gamma_y\\
&+\kappa_0\int_\Gamma \left[\bar{\theta}(\boldsymbol{y},p)-\bar{\theta}(\boldsymbol{x},p)\right]\,\bar{F}(\boldsymbol{x},\boldsymbol{y},p)d\Gamma_y\\
&-\kappa_0\int_\Gamma \frac{\tilde{k}(\boldsymbol{y})}{\tilde{E}(\boldsymbol{y})\tilde{\alpha}(\boldsymbol{y})}\,\bar{q}(\boldsymbol{y},p)\,\bar{T}(\boldsymbol{x},\boldsymbol{y},p)d\Gamma_y \qquad (14)\\
&+\frac{\kappa_0\eta_0 p}{\gamma_0}\int_\Gamma \left[\frac{1}{\tilde{E}(\boldsymbol{y})\tilde{\alpha}(\boldsymbol{y})}\,\bar{t}_i(\boldsymbol{y},p)\,\bar{U}_i(\boldsymbol{x},\boldsymbol{y},p)\right.\\
&\left.-\bar{u}_i(\boldsymbol{y},p)\,\bar{T}_i(\boldsymbol{x},\boldsymbol{y},p)\right]d\Gamma_y-\bar{F}^{(\theta)}(\boldsymbol{x},p)=0.
\end{aligned}$$

In this manner the BDIEs (13) and (14) are free from the Cauchy principal value integrals. The first integrals on the left-side of Eqs. (13) and (14) become weakly singular with static thermoelastic fundamental solutions. The second integrals are regular at $|\boldsymbol{y}-\boldsymbol{x}|\to 0$. To deal with the weak singularity suitable regularization schemes for the boundary and for the domain integrals [Aliabadi (2002)] are utilized. Thus, all integrals in Eqs. (13) and (14) are now regular which can be computed numerically by using standard Gaussian quadrature formula.

Supplementing the BDIEs (13) and (14) with the domain integral equations (8) and (9) we obtain a system of integral equations for the boundary unknowns and the displacement and temperature fields at internal points.

3 Numerical solution procedure

In order to solve the system of boundary-domain integral equations an efficient BDEM is developed. A collocation method is employed for the spatial discretiza-

tion of the equations in the Laplace-transformed domain. The boundary Γ is divided into N^b quadratic boundary elements Γ_q and the interior of the domain Ω into N^d the quadrilateral domain elements Ω_g. Every node within the boundary Γ_q or the domain element Ω_g is numbered by a local number $a = 1,2,3$ or $s = 1,\ldots,8$, respectively. The Cartesian coordinates of the interior points on the elements are parametrically expressed as

$$x_i|_{\boldsymbol{x}\in\Gamma_q} = \sum_{a=1}^{3} x_i^{w(q,a)} N^a(\xi),$$

$$x_i|_{\boldsymbol{x}\in\Omega_g} = \sum_{s=1}^{8} x_i^{v(g,s)} N^s(\xi_1,\xi_2),$$

where $x_i^{w(q,a)}$ and $x_i^{v(g,s)}$ are the Cartesian coordinates of the a-th nodal point on Γ_q and the s-th nodal point on Ω_g, respectively, $N^a(\xi)$ and $N^s(\xi_1,\xi_2)$ represent the shape functions [Aliabadi (2002)]. In addition to the local numeration the global numeration of the boundary nodes $w(q,a)$, $1 \le w \le W$ and the internal nodes $v(g,s)$, $1 \le v \le V$ is employed, with W and V being the total numbers of the boundary and internal nodes, respectively. A polynomial approximation for the unknown field quantities within the introduced elements Γ_q and Ω_g is employed

$$\bar{f}(\boldsymbol{x},p)|_{\boldsymbol{x}\in\Gamma_q} = \sum_{a=1}^{3} \bar{f}(\boldsymbol{x}^{w(q,a)},p) N^a(\xi),$$

$$\bar{f}(\boldsymbol{x},p)|_{\boldsymbol{x}\in\Omega_g} = \sum_{s=1}^{8} \bar{f}(\boldsymbol{x}^{v(g,s)},p) N^s(\xi_1,\xi_2),$$

where $\bar{f}$ corresponds to $\bar{u}_i$, $\bar{t}_i$, $\bar{\theta}$ or $\bar{q}$.

Applying the BDIEs (8),(9), (13) and (14) at all collocation nodes and replacing the integrals over the boundary Γ and the domain Ω by the sum of integrals over the boundary element Γ_q and the element area Ω_g we obtain a system of $3N$ ($N = W+V$) linear algebraic equations for the unknown field quantities at the collocation points. After numerical integrations, invoking the prescribed boundary conditions the system of linear algebraic equations can be written as

$$\boldsymbol{A}^b\boldsymbol{x}^b = \boldsymbol{y}^b + \boldsymbol{V}^b\boldsymbol{u}, \qquad \text{for boundary nodes,} \tag{15}$$

$$\boldsymbol{A}^i\boldsymbol{x}^b + \boldsymbol{u}^i = \boldsymbol{y}^i - \boldsymbol{V}^i\boldsymbol{u}, \qquad \text{for internal nodes,} \tag{16}$$

where the superscripts b or i denote a quantity at a boundary point or at an interior point. In Eqs. (15) and (16), the vector $\boldsymbol{x}^b$ with a size of $3W$ contains the boundary unknowns, while the vector $\boldsymbol{u}^i$ with a size of $3V$ consists of the unknown internal

displacements and temperature. The vector $\boldsymbol{u}$ with a size of $3N$ is composed of the vectors $\boldsymbol{x}^b$ and $\boldsymbol{u}^i$, $\boldsymbol{y}^b$ and $\boldsymbol{y}^i$ denote $3W$ and $3V$ vectors of the prescribed boundary displacements, tractions, temperature and heat flux. The sizes of the matrices $\boldsymbol{A}^b$ and $\boldsymbol{A}^i$ are $3W \times 3W$ and $3V \times 3W$, while $\boldsymbol{V}^b$ and $\boldsymbol{V}^i$ are $3W \times 3N$ and $3V \times 3N$, respectively.

The system of linear algebraic equations (15) and (16) can be rewritten into the following matrix form

$$\left(\begin{bmatrix} \boldsymbol{A}^b & 0 \\ \boldsymbol{A}^i & \boldsymbol{I} \end{bmatrix} - \begin{bmatrix} \boldsymbol{V}^b \\ \boldsymbol{V}^i \end{bmatrix} \right) \begin{bmatrix} \boldsymbol{x}^b \\ \boldsymbol{u}^i \end{bmatrix} = \begin{bmatrix} \boldsymbol{y}^b \\ \boldsymbol{y}^i \end{bmatrix}, \tag{17}$$

where $\boldsymbol{I}$ is the identity matrix. The system (17) is solved numerically for discrete values of the Laplace-transform parameter p to obtain the boundary unknowns $\boldsymbol{x}^b$ and the internal primary fields $\boldsymbol{u}^i$.

The time-dependent solutions can be calculated by an inverse Laplace-transform that is an ill-posed problem, because small truncation errors may be accumulated in the inversion process. There are many numerical inversion methods and their comparative analysis can be found in [Davies and Martin (1979)]. In the present paper, the Stehfest's algorithm is employed [Stehfest (1970)], from which an approximated value f_a of a function f for a specific time t can be computed as

$$f_a(t) = \frac{\ln 2}{t} \sum_{i=1}^{N_s} v_i \bar{f}\left(\frac{\ln 2}{t} i \right), \tag{18}$$

where

$$v_i = (-1)^{N_s/(i+2)} \times \sum_{k=[(i+1)/2]}^{\min(i,N_s/2)} \frac{k^{N_s/2}\,(2k)!}{(N_s/2-k)!\,k!\,(k-1)!\,(i-k)!\,(2k-i)!}.$$

For each time instant, we solve N_s boundary value problems in the Laplace-transformed domain for the corresponding transform parameter $p = i \ln 2/t$. Stehfest (1970) has suggested to use $N_s = 10$ for single and $N_s = 18$ for double precision arithmetic. In the present analysis $N_s = 18$ is adopted and in this case we obtain numerical results comparable with those computed by Durbin's method [Durbin (1974)] that requires a complex arithmetic and more computing time to achieve the convergence.

4 Computation of the stress intensity factors

Different methods can be used for the evaluation of stress intensity factors [Buchholz, Grebner, and Strathmeier (1986); Dhondt, Chergui, and Buchholz (2001)].

In this analysis, the extrapolation technique following directly from the asymptotic expansion of the displacements in the vicinity of the crack-tip is employed [Aliabadi (2002); Sládek, Sládek, and Zhang (2005)]. The asymptotic stress and displacement fields near the crack-tip in continuously non-homogeneous and linear elastic FGMs have the same singularity and structure as those in homogeneous and linear elastic materials [Eischen (1987); Erdogan (1995)].

The dynamic stress intensity factors are related to the crack-opening-displacements $\Delta u_i(\varepsilon,t)$ by

$$\begin{Bmatrix} K_{\mathrm{I}}(t) \\ K_{\mathrm{II}}(t) \end{Bmatrix} = \frac{\sqrt{2\pi}}{\kappa+1}\mu^{\mathrm{tip}} \lim_{\varepsilon\to 0} \frac{1}{\sqrt{a-\varepsilon}} \begin{Bmatrix} \Delta u_2(\varepsilon,t) \\ \Delta u_1(\varepsilon,t) \end{Bmatrix}, \tag{19}$$

with

$$\kappa = \begin{cases} 3-4\nu, & \text{for plane strain,} \\ \dfrac{3-\nu}{1+\nu}, & \text{for plane stress,} \end{cases}$$

where $K_{\mathrm{I}}(t)$ and $K_{\mathrm{II}}(t)$ represent the mode-I and mode-II dynamic stress intensity factors, μ^{tip} is the shear modulus at the crack-tip and ε is a small distance from the crack-tip to the considered node on the crack-faces.

5 Numerical examples

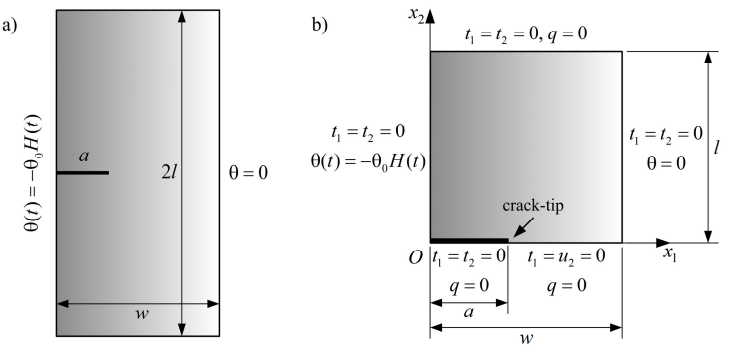

Figure 1: An edge crack in a rectangular FGM plate under thermal shock

An edge crack in a rectangular, isotropic, continuously non-homogeneous and linear elastic FGM plate is considered. The plate geometry is described by the width $w = 1$, length $2l = 3w$ and the crack length $a = 0.4w$ (Fig. 1). The cracked plate is subjected to a cooling thermal shock $\theta(\boldsymbol{x},t) = -\theta_0 H(t)$ at the lateral side, where

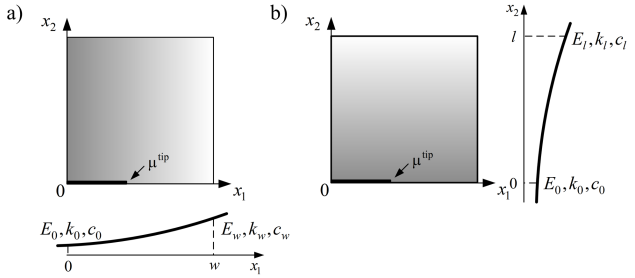

Figure 2: FGM plate with the material gradation in the x_1-direction (a) and in the x_2-direction (b)

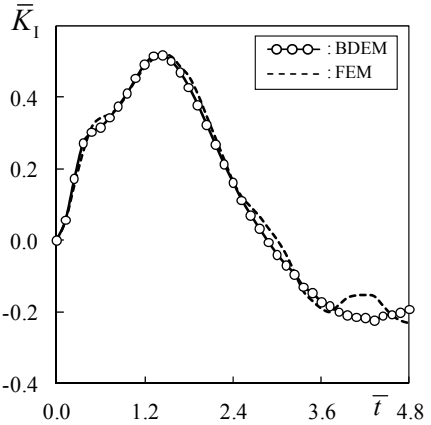

Figure 3: Normalized mode-I dynamic SIF for the homogeneous cracked plate

θ_0 is the constant amplitude and $H(t)$ is the Heaviside step function. The material gradation in the x_i-direction is assumed to have an exponential gradation

$$\begin{aligned} E(x_i) &= E_0 \exp(\alpha_g |x_i|), \\ k(x_i) &= k_0 \exp(\beta_g |x_i|), \\ c(x_i) &= c_0 \exp(\gamma_g |x_i|), \end{aligned} \tag{20}$$

with

$$\alpha_g = \frac{1}{\ell} \ln\left(\frac{E_b}{E_0}\right), \qquad \beta_g = \frac{1}{\ell} \ln\left(\frac{k_b}{k_0}\right), \gamma_g = \frac{1}{\ell} \ln\left(\frac{c_b}{c_0}\right),$$

where $E_0 = E(0)$, $k_0 = k(0)$, $c_0 = c(0)$ and $E_b = E(\ell)$, $k_b = k(\ell)$, $c_b = c(\ell)$; ℓ is either equal to w or to l for the material gradation in the x_1- (Fig. 2a) or in

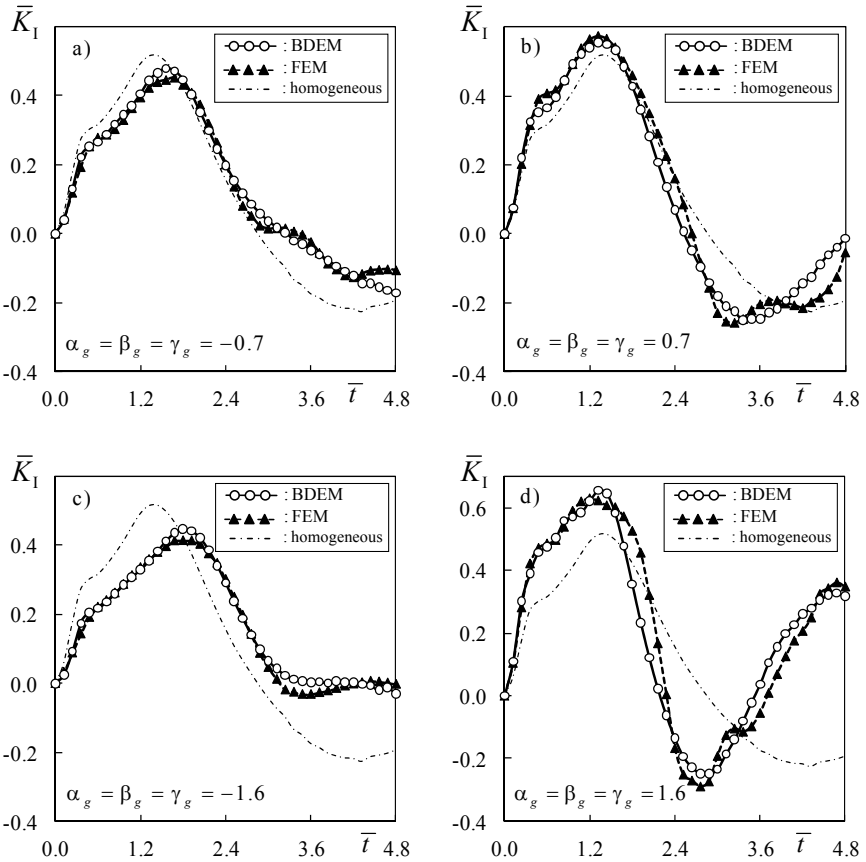

Figure 4: Time variations of the dynamic SIF for the material gradation in the x_1-direction

the x_2-direction (Fig. 2b), respectively. The mass density, the Poisson's ratio and the linear thermal expansion coefficient are taken as constant $\rho(\boldsymbol{x}) = 1$, $\nu = 0.25$ and $\alpha(\boldsymbol{x}) = 0.02$, respectively. Plane strain condition is assumed in the numerical analysis.

Due to the selected material gradations, the symmetry of the loading conditions and the plate geometry only one half of the plate is considered in the numerical computations. In this case, the mode-I dynamic stress intensity factor occurs whereas the mode-II stress intensity factor is identically zero. In the plate discretization, 80 boundary and 341 interior nodes are used. The displacement and temperature fields are modelled by 40 three-node quadratic boundary and 100 eight-node quadrilateral domain elements. For convenience, the dynamic stress intensity factor and time are

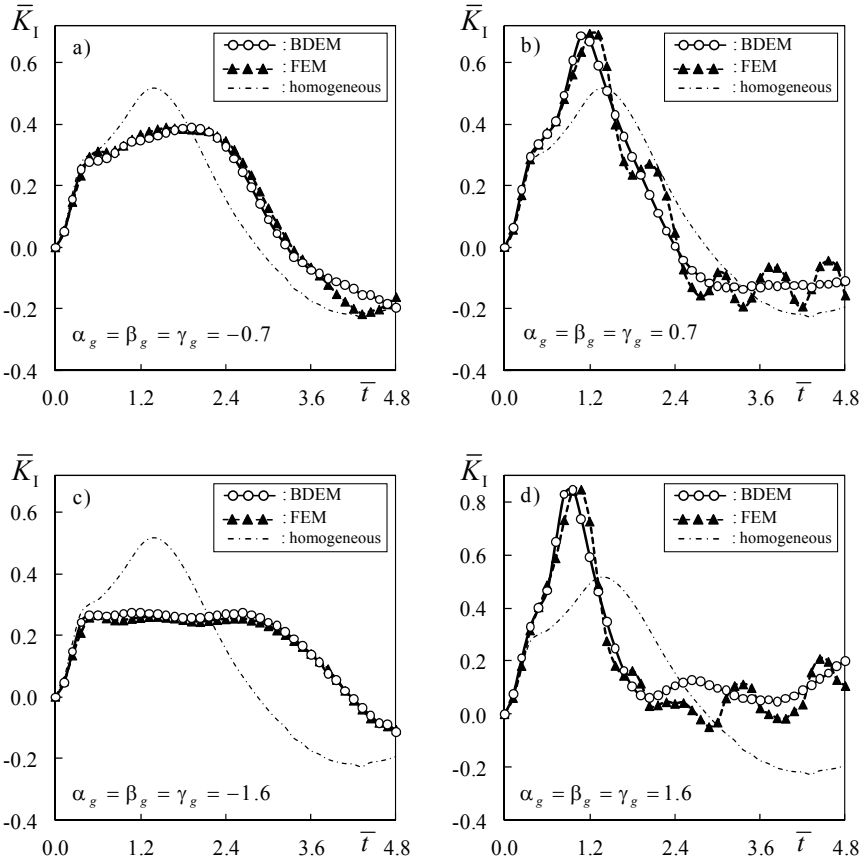

Figure 5: Time variations of the dynamic SIF for the material gradation in the x_2-direction

normalized as $\bar{K}_I(t) = K_I(t)/\alpha_0 E_0 \theta_0 \sqrt{\pi a}$ and $\bar{t} = t\, k_0/a^2 \rho_0 c_0$.

To test the accuracy of the proposed method we consider a homogeneous plate with $\alpha_g = \beta_g = \gamma_g = 0$. The temporal variation of the normalized mode-I dynamic stress intensity factor is presented in Fig. 3. The corresponding numerical result obtained by FEM using FEMLAB code (dashed line) is also shown in Fig. 3. A comparison of both numerical methods shows a good agreement.

After the verification of the accuracy we investigate the influence of the material gradation on the cracked FGM plate. The material parameters are the same as in the previous homogeneous case. Four material gradient parameters $\alpha_g = \beta_g = \gamma_g = \pm 0.7, \pm 1.6$ are selected. The material gradation in the x_1-direction parallel to the crack-line (Fig. 2a) is first considered. The time variations of the normal-

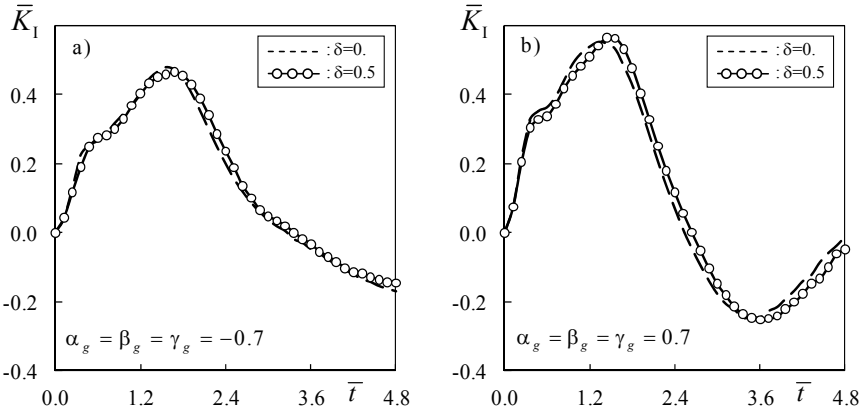

Figure 6: Effect of thermo-mechanical coupling on the time variations of normalized mode-I dynamic SIF for the non-homogeneous cracked plate

ized mode-I dynamic stress intensity factor for the chosen gradient parameters are shown Fig. 4. The numerical results obtained by the BDEM and FEM agree very well. For comparison purpose, the curve of the normalized mode-I dynamic stress intensity factor for the cracked homogeneous plate (dot-dashed line) is also plotted in Fig. 4. The first peak of the normalized mode-I dynamic stress intensity factor is reduced with the decreasing gradient parameters, see Fig. 4a and Fig. 4c. In contrast to the homogeneous material, the peak values of the stress intensity factors are reached at larger time instants because the velocity of the wave propagation is lower. The opposite tendency takes place for an increase of the gradient parameters, see Fig. 4b and Fig. 4d. The first peak of the stress intensity factor is enhanced in comparison with homogeneous case.

Next, the material gradation of the FGM plate perpendicular to the crack-line (Fig. 2b) is considered for the same gradient parameters. Fig. 5 shows the time variations of the normalized mode-I dynamic stress intensity factor. One can see a quite good agreement of the numerical results obtained by the BDEM and the FEM. A similar trend as in the previous example can be observed. The first peaks of the normalized mode-I dynamic stress intensity factor for the negative gradient parameters (Fig. 5a and Fig. 5c) are smaller than those for an edge crack parallel to the material gradation (Fig. 4a and Fig. 4c). On the contrary, for the positive gradient parameters they are significantly larger and reached at smaller time instants than those for the material gradation in the x_1-direction, see Fig. 5b, Fig. 5d and Fig. 4b, Fig. 4d. From Fig. 4 and Fig. 5 we can conclude that the peak values of the normalized mode-I dynamic stress intensity factor and the time instants, at which they occur,

depend significantly on the direction of the material gradation and the values of the gradient parameters.

Finally, we consider a cracked FGM plate with material gradation in the x_1-direction (Fig. 2a) using the coupled theory of thermoelasticity. A measure of the thermo-mechanical coupling can be described by

$$\delta(\boldsymbol{x}) = \frac{(1+\nu)}{(1-\nu)(1-2\nu)} \frac{\alpha^2(\boldsymbol{x}) E(\boldsymbol{x}) T_0}{\rho(\boldsymbol{x}) c(\boldsymbol{x})} \tag{21}$$

that equals zero for an uncoupled problem, such as in the above examples. The coupled parameter is taken as constant $\delta(\boldsymbol{x}) = 0.5$ and corresponds to the previously used material parameters with the reference temperature $T_0 = 375$. The time variations of the normalized mode-I stress intensity factor for the gradient parameters $\alpha_g = \beta_g = \gamma_g = \pm 0.7$ in coupled and uncoupled cases are shown in Fig. 6. For both gradient parameters, the position of the peaks of the stress intensity factor is slightly shifted to the larger time instants compared to the uncoupled case, because the wave propagation velocity is reduced. The thermo-mechanical coupling has a minimal influence on the dynamic stress intensity factors regardless of the value of the selected gradient parameters.

6 Conclusions

A 2-D transient thermoelastic crack analysis in isotropic, non-homogeneous and linear elastic FGMs subjected to a thermal shock is presented in this paper. For this purpose, a boundary-domain element method is proposed. Fundamental solutions of linear coupled thermoelasticity for the corresponding homogeneous, isotropic and linear elastic materials in the Laplace-transformed domain are employed to derive the boundary-domain integral equation formulations. The material non-homogeneity is described by additional domain integrals, which require a special regularization and domain discretization. A collocation-based BDEM is developed in the Laplace-transformed domain. The numerical inversion of the Laplace-transform is performed by using the Stehfest's algorithm. For an edge crack in a 2-D FGM plate, the time variations of the dynamic stress intensity factors are presented and discussed. Numerical results obtained by the BDEM show a good agreement with those obtained by the FEM. The dynamic SIFs may be significantly affected by the material gradation and the thermo-mechanical coupling. The present BDEM can be easily extended to crack problems with an arbitrarily-oriented crack by using the sub-domain technique.

Acknowledgement: This work is supported by the German Research Foundation (DFG, Project No.: ZH 15/10-2), which is gratefully acknowledged.

References

Aliabadi, M. H. (2002): *The Boundary Element Method: Applications in Solids and Structures*, volume 2. John Wiley & Sons, Baffins Lane, Chichester.

Anlas, G.; Santare, M. H.; Lambros, J. (2000): Numerical calculation of stress intensity factors in functionally graded materials. *International Journal of Fracture*, vol. 104, no. 2, pp. 131–143.

Balaš, J.; Sládek, J.; Sládek, V. (1989): *Stress Analysis by Boundary Element Methods*. Elsevier, Amsterdam.

Batra, R. C.; Love, B. M. (2005): Crack propagation due to brittle and ductile failures in microporous thermoelastoviscoplastic functionally graded materials. *Engineering Fracture Mechanics*, vol. 72, no. 12, pp. 1954–1979.

Buchholz, F.-G.; Grebner, H.; Strathmeier, U. (1986): Numerical investigations of crack closure integral and J-integral calculations for a thermally stressed specimen. *International Journal of Solids and Structures*, vol. 22, no. 7, pp. 709 – 719.

Chen, J.; Dargush, G. F. (1995): Boundary element method for dynamic poroelastic and thermoelastic analyses. *International Journal of Solids and Structures*, vol. 32, no. 15, pp. 2257–2278.

Citarella, R.; Buchholz, F.-G. (2008): Comparison of crack growth simulation by DBEM and FEM for SEN-specimens undergoing torsion or bending loading. *Engineering Fracture Mechanics*, vol. 75, no. 3-4, pp. 489 – 509.

Dag, S.; Yildirim, B. (2009): Computation of thermal fracture parameters for inclined cracks in functionally graded materials using J_k-Integral. *Journal of Thermal Stresses*, vol. 32, no. 5, pp. 530–556.

Dargush, G.; Banerjee, P. (1989): Development of a boundary element method for time-dependent planar thermoelasticity. *International Journal of Solids and Structures*, vol. 25, no. 9, pp. 999–1021.

Dargush, G. F.; Banerjee, P. K. (1990): Boundary element methods in three-dimensional thermoelasticity. *International Journal of Solids and Structures*, vol. 26, no. 2, pp. 199–216.

Dargush, G. F.; Banerjee, P. K. (1991): A new boundary element method for three-dimensional coupled problems of consolidation and thermoelasticity. *Transaction of the ASME Journal of Applied Mechanics*, vol. 58, pp. 28–36.

Davies, B.; Martin, B. (1979): Numerical inversion of the Laplace transform: A survey and comparison of methods. *Journal of Computational Physics*, vol. 33, no. 1, pp. 1–32.

Dhondt, G.; Chergui, A.; Buchholz, F. G. (2001): Computational fracture analysis of different specimens regarding 3D and mode coupling effects. *Engineering Fracture Mechanics*, vol. 68, no. 4, pp. 383 – 401.

Ding, S.-H.; Li, X. (2010): Thermal stress intensity factors for an interface crack in a functionally graded layered structures. *Archive of Applied Mechanics*, pp. 1–13.

Durbin, F. (1974): Numerical inversion of Laplace transforms: An efficient improvement to Dubner and Abate's method. *The Computer Journal*, vol. 17, no. 4, pp. 371–376.

Eischen, J. W. (1987): Fracture of nonhomogeneous materials. *International Journal of Fracture*, vol. 34, no. 1, pp. 3–22.

Erdogan, F. (1995): Fracture mechanics of functionally graded materials. *Composites Engineering*, vol. 5, no. 7, pp. 753–770.

Erdogan, F.; Rizk, A. A. (1992): Fracture of coated plates and shells under thermal shock. *International Journal of Fracture*, vol. 53, no. 2, pp. 159–185.

Erdogan, F.; Wu, B. H. (1996): Crack problems in FGM layers under thermal stresses. *Journal of Thermal Stresses*, vol. 19, no. 3, pp. 237–265.

Fujimoto, T.; Noda, N. (2000): Crack propagation in a functionally graded plate under thermal shock. *Archive of Applied Mechanics*, vol. 70, no. 6, pp. 377–386.

Fujimoto, T.; Noda, N. (2001): Two crack growths in a functionally graded plate under thermal shock. *Journal of Thermal Stresses*, vol. 24, no. 9, pp. 847–862.

Gao, X.; Zhang, C.; Sladek, J.; Sladek, V. (2008): Fracture analysis of functionally graded materials by a BEM. *Composites Science and Technology*, vol. 68, no. 5, pp. 1209–1215.

Guo, L.-C.; Noda, N. (2010): An analytical method for thermal stresses of a functionally graded material cylindrical shell under a thermal shock. *Acta Mechanica*, vol. 214, no. 1, pp. 71–78.

Hosseini-Tehrani, P.; Eslami, M. R. (2000): BEM analysis of thermal and mechanical shock in a two-dimensional finite domain considering coupled thermoelasticity. *Engineering Analysis with Boundary Elements*, vol. 24, no. 3, pp. 249–257.

Hosseini-Tehrani, P.; Eslami, M. R.; Daghyani, H. R. (2001): Dynamic crack analysis under coupled thermoelastic assumption. *Journal of Applied Mechanics*, vol. 68, no. 4, pp. 584–588.

Hosseini-Tehrani, P.; Hosseini-Godarzi, A.; Tavangar, M. (2005): Boundary element analysis of stress intensity factor K_I in some two-dimensional dynamic

thermoelastic problems. *Engineering Analysis with Boundary Elements*, vol. 29, no. 3, pp. 232–240.

Hosseini-Tehrani, P.; Hosseini-Godarzi, A. R. (2004): Dynamic crack analysis under thermal shock considering Lord-Shulman theory. *International Journal of Thermal Sciences*, vol. 43, no. 10, pp. 1003–1010.

Jin, Z. H. (2004): Effect of thermal property gradients on the edge cracking in a functionally graded coating. *Surface and Coatings Technology*, vol. 179, no. 2-3, pp. 210–214.

Jin, Z.-H.; Noda, N. (1994): Edge crack in a nonhomogeneous half plane under thermal loading. *Journal of Thermal Stresses*, vol. 17, no. 4, pp. 591–599.

Jin, Z. H.; Paulino, G. H. (2001): Transient thermal stress analysis of an edge crack in a functionally graded material. *International Journal of Fracture*, vol. 107, no. 1, pp. 73–98.

Katsareas, D. E.; Anifantis, N. K. (1995): On the computation of mode I and II thermal shock stress intensity factors using a boundary-only element method. *International Journal for Numerical Methods in Engineering*, vol. 38, no. 24, pp. 4157–4169.

Kim, J.-H.; Paulino, G. H. (2003): Mixed-mode J-integral formulation and implementation using graded elements for fracture analysis of nonhomogeneous orthotropic materials. *Mechanics of Materials*, vol. 35, no. 1-2, pp. 107–128.

Kim, J. H.; Paulino, G. H. (2005): Consistent formulations of the interaction integral method for fracture of functionally graded materials. *Journal of Applied Mechanics*, vol. 72, no. 3, pp. 351–364.

Kögl, M.; Gaul, L. (2000): A dual reciprocity boundary element method for dynamic coupled anisotropic thermoelasticity. In Jentsch, L.; Tröltzsch, F.(Eds): *Boundary Elements XXII*, pp. 565–577. WIT Press Southampton, Southampton.

Kögl, M.; Gaul, L. (2003): A boundary element method for anisotropic coupled thermoelasticity. *Archive of Applied Mechanics*, vol. 73, no. 5-6, pp. 377–398.

Lee, Y. D.; Erdogan, F. (1994): Residual/thermal stresses in FGM and laminated thermal barrier coatings. *International Journal of Fracture*, vol. 69, no. 2, pp. 145–165.

Lu, Y. L.; Liu, H.; Jia, H.; Yu, Z. Q. (2001): Finite element implementation of thermal weight function method for calculating transient SIFs of a body subjected to thermal shock. *International Journal of Fracture*, vol. 108, no. 2, pp. 95–117.

Nemat-Alla, M.; Noda, N. (1996): Thermal stress intensity factor for functionally gradient half space with an edge crack under thermal load. *Archive of Applied Mechanics*, vol. 66, no. 8, pp. 569–580.

Nemat-Alla, M.; Noda, N. (2000): Edge crack problem in a semi-infinite FGM plate with a bi-directional coefficient of thermal expansion under two-dimensional thermal loading. *Acta Mechanica*, vol. 144, no. 3, pp. 211–229.

Noda, N.; Ashida, F.; Matsunaga, Y. (1994): Stress intensity factors for external and penny-shaped cracks in transversely isotropic cylinders subjected to thermal shock. *Archive of Applied Mechanics*, vol. 64, no. 6, pp. 383–394.

Noda, N.; Guo, L. C. (2008): Thermal shock analysis for a functionally graded plate with a surface crack. *Acta Mechanica*, vol. 195, no. 1, pp. 157–166.

Noda, N.; Ishihara, M.; Yamamoto, N.; Fujimoto, T. (2003): Two-cracks propagation problem in a functionally graded material plate under thermal loads. *Materials Science Forum*, vol. 423-425, pp. 607–612.

Paulino, G. H.; Jin, Z. H.; Dodds, R. H. J. (2003): Failure of functionally graded materials. In Milne, I.; Ritchie, R. O.; Karihaloo, B.(Eds): *Comprehensive Structural Integrity*, volume 2, chapter 13, pp. 607–644. Pergamon, Oxford.

Santare, M. H.; Lambros, J. (2000): Use of graded finite elements to model the behavior of nonhomogeneous materials. *Journal of Applied Mechanics*, vol. 67, no. 4, pp. 819–822.

Sládek, J.; Sládek, V.; Markechova, I. (1990): Boundary element method analysis of stationary thermoelasticity problems in non-homogeneous media. *International Journal for Numerical Methods in Engineering*, vol. 30, no. 3, pp. 505–516.

Sládek, J.; Sládek, V.; Solek, P.; Tan, C.; Zhang, C. (2009): Two- and three-dimensional transient thermoelastic analysis by the MLPG method. *Computer Modeling in Engineering & Sciences*, vol. 47, no. 1, pp. 61–96.

Sládek, J.; Sládek, V.; Zhang, C. (2005): An advanced numerical method for computing elastodynamic fracture parameters in functionally graded materials. *Computational Materials Science*, vol. 32, no. 3-4, pp. 532–543.

Sládek, J.; Sládek, V.; Zhang, C.; Tan, C. L. (2006): Meshless local Petrov-Galerkin method for linear coupled thermoelastic analysis. *Computer Modeling in Engineering & Sciences*, vol. 16, no. 1, pp. 57–68.

Sládek, V.; Sládek, J.; Markechova, I. (1993): An advanced boundary element method for elasticity problems in nonhomogeneous media. *Acta Mechanica*, vol. 97, no. 1, pp. 71–90.

Stehfest, H. (1970): Algorithm 368: Numerical inversion of Laplace transform. *Communications of the ACM*, vol. 13, no. 1, pp. 47–49.

Suresh, S.; Mortensen, A. (1998): *Fundamentals of Functionally Gradient Materials*. The Institute of Materials, IOM Communications Ltd., London, London.

Tanaka, M.; Matsumoto, T.; Moradi, M. (1995): Application of boundary element method to 3-D problems of coupled thermoelasticity. *Engineering Analysis with Boundary Elements*, vol. 16, no. 4, pp. 297–303.

Tehrani, P. H.; Eslami, M. R. (1998): Two-dimensional time-harmonic dynamic coupled thermoelasticity analysis by boundary element method formulation. *Engineering Analysis with Boundary Elements*, vol. 22, no. 3, pp. 245–250.

Tosaka, N.; Suh, I. G. (1991): Boundary element analysis of dynamic coupled thermoelasticity problems. *Computational Mechanics*, vol. 8, no. 5, pp. 331–342.

Yildirim, B. (2006): An equivalent domain integral method for fracture analysis of functionally graded materials under thermal stresses. *Journal of Thermal Stresses*, vol. 29, no. 4, pp. 371–397.

Yildirim, B.; Erdogan, F. (2004): Edge crack problems in homogenous and functionally graded material thermal barrier coatings under uniform thermal loading. *Journal of Thermal Stresses*, vol. 27, no. 4, pp. 311–329.

Zamani, A.; Reza Eslami, M. (2009): Coupled dynamical thermoelasticity of a functionally graded cracked layer. *Journal of Thermal Stresses*, vol. 32, no. 10, pp. 969–985.

Appendix A: Functions $\bar{F}_j^{(u)}$ and $\bar{F}^{(\theta)}$

The functions $\bar{F}_j^{(u)}$ and $\bar{F}^{(\theta)}$ in Eqs. (8), (9), (13) and (14) are defined by the following domain integrals

$$\begin{aligned}\bar{F}_j^{(u)}(\boldsymbol{x},p) = p^2\rho_0 \int_\Omega f_{ij}^{(1)}(\boldsymbol{x},\boldsymbol{y},p)\bar{u}_i(\boldsymbol{y},p)d\Omega_y \\ +\mu_0 \int_\Omega f_{ijk}^{(2)}(\boldsymbol{x},\boldsymbol{y},p)\bar{u}_{i,k}(\boldsymbol{y},p)d\Omega_y \\ + \int_\Omega f_j^{(3)}(\boldsymbol{x},\boldsymbol{y},p)\bar{\theta}(\boldsymbol{y},p)d\Omega_y \\ +\kappa_0 \int_\Omega f_{ij}^{(4)}(\boldsymbol{x},\boldsymbol{y},p)\bar{\theta}_{,i}(\boldsymbol{y},p)d\Omega_y,\end{aligned} \tag{22}$$

$$\begin{aligned}\bar{F}^{(\theta)}(\boldsymbol{x},p) &= p^2\rho_0\int_\Omega f_i^{(5)}(\boldsymbol{x},\boldsymbol{y},p)\bar{u}_i(\boldsymbol{y},p)d\Omega_y \\ &+\mu_0\int_\Omega f_{ij}^{(6)}(\boldsymbol{x},\boldsymbol{y},p)\bar{u}_{i,j}(\boldsymbol{y},p)d\Omega_y \\ &+p\int_\Omega f^{(7)}(\boldsymbol{x},\boldsymbol{y},p)\bar{\theta}(\boldsymbol{y},p)d\Omega_y \\ &+\kappa_0\int_\Omega f_i^{(8)}(\boldsymbol{x},\boldsymbol{y},p)\bar{\theta}_{,i}(\boldsymbol{y},p)d\Omega_y,\end{aligned} \tag{23}$$

with additional functions

$$f_{ij}^{(1)}(\boldsymbol{x},\boldsymbol{y},p) = -\left(\frac{\tilde{\rho}(\boldsymbol{y})}{\tilde{E}(\boldsymbol{y})\tilde{\alpha}(\boldsymbol{y})}-1\right)\bar{U}_{ij}(\boldsymbol{x},\boldsymbol{y},p),$$

$$\begin{aligned}f_{ijk}^{(2)}(\boldsymbol{x},\boldsymbol{y},p) &= \frac{2(1-\nu)}{1-2\nu}\frac{1}{\tilde{\alpha}(\boldsymbol{y})}\left(\frac{\tilde{E}_{,j}(\boldsymbol{y})}{\tilde{E}(\boldsymbol{y})}\right. \\ &\left.+\frac{\tilde{\alpha}_{,j}(\boldsymbol{y})}{\tilde{\alpha}(\boldsymbol{y})}\right)\bar{U}_{ik}(\boldsymbol{x},\boldsymbol{y},p)-\left(\frac{1}{\tilde{\alpha}(\boldsymbol{y})}-1\right) \\ &\times\left(\frac{1}{1-2\nu}\bar{U}_{ij,k}(\boldsymbol{x},\boldsymbol{y},p)+\bar{U}_{kj,i}(\boldsymbol{x},\boldsymbol{y},p)\right),\end{aligned}$$

$$\begin{aligned}f_j^{(3)}(\boldsymbol{x},\boldsymbol{y},p) &= p\left(\frac{\tilde{\rho}(\boldsymbol{y})\tilde{c}(\boldsymbol{y})}{\tilde{E}(\boldsymbol{y})\tilde{\alpha}(\boldsymbol{y})}-1\right)\bar{U}_j(\boldsymbol{x},\boldsymbol{y},p) \\ &-\gamma_0\left(\frac{\tilde{E}_{,j}(\boldsymbol{y})}{\tilde{E}(\boldsymbol{y})}+\frac{\tilde{\alpha}_{,j}(\boldsymbol{y})}{\tilde{\alpha}(\boldsymbol{y})}\right)\bar{U}_{kk}(\boldsymbol{x},\boldsymbol{y},p),\end{aligned}$$

$$\begin{aligned}f_{ij}^{(4)}(\boldsymbol{x},\boldsymbol{y},p) &= \left(\frac{\tilde{k}(\boldsymbol{y})}{\tilde{E}(\boldsymbol{y})\tilde{\alpha}(\boldsymbol{y})}-1\right)\bar{U}_{j,i}(\boldsymbol{x},\boldsymbol{y},p)- \\ &-\frac{1}{\eta_0}\frac{\tilde{k}(\boldsymbol{y})}{\tilde{E}(\boldsymbol{y})\tilde{\alpha}(\boldsymbol{y})}\left(\frac{\tilde{E}_{,i}(\boldsymbol{y})}{\tilde{E}(\boldsymbol{y})}+\frac{\tilde{\alpha}_{,i}(\boldsymbol{y})}{\tilde{\alpha}(\boldsymbol{y})}\right)\bar{U}_j(\boldsymbol{x},\boldsymbol{y},p),\end{aligned}$$

$$f_i^{(5)}(\boldsymbol{x},\boldsymbol{y},p) = \frac{\kappa_0\eta_0 p}{\gamma_0}\left(\frac{\tilde{\rho}(\boldsymbol{y})}{\tilde{E}(\boldsymbol{y})\tilde{\alpha}(\boldsymbol{y})}-1\right)\bar{U}_i(\boldsymbol{x},\boldsymbol{y},p),$$

$$\begin{aligned}f_{ij}^{(6)}(\boldsymbol{x},\boldsymbol{y},p) &= \frac{\kappa_0\eta_0 p}{\gamma_0}\left[-\frac{2(1-\nu)}{1-2\nu}\frac{1}{\tilde{\alpha}(\boldsymbol{y})}\left(\frac{\tilde{E}_{,j}(\boldsymbol{y})}{\tilde{E}(\boldsymbol{y})}\right.\right. \\ &\left.+\frac{\tilde{\alpha}_{,j}(\boldsymbol{y})}{\tilde{\alpha}(\boldsymbol{y})}\right)\bar{U}_i(\boldsymbol{x},\boldsymbol{y},p)+\left(\frac{1}{\tilde{\alpha}(\boldsymbol{y})}-1\right) \\ &\left.\times\left(\frac{1}{1-2\nu}\bar{U}_{i,j}(\boldsymbol{x},\boldsymbol{y},p)+\bar{U}_{j,i}(\boldsymbol{x},\boldsymbol{y},p)\right)\right],\end{aligned}$$

$$f^{(7)}(\boldsymbol{x},\boldsymbol{y},p) = -\left(\frac{\tilde{\rho}(\boldsymbol{y})\tilde{c}(\boldsymbol{y})}{\tilde{E}(\boldsymbol{y})\tilde{\alpha}(\boldsymbol{y})} - 1\right)\bar{T}(\boldsymbol{x},\boldsymbol{y},p)$$
$$+ \kappa_0\eta_0\left(\frac{\tilde{E}_{,j}(\boldsymbol{y})}{\tilde{E}(\boldsymbol{y})} + \frac{\tilde{\alpha}_{,j}(\boldsymbol{y})}{\tilde{\alpha}(\boldsymbol{y})}\right)\bar{U}_j(\boldsymbol{x},\boldsymbol{y},p),$$
$$f_i^{(8)}(\boldsymbol{x},\boldsymbol{y},p) = -\left(\frac{\tilde{k}(\boldsymbol{y})}{\tilde{E}(\boldsymbol{y})\tilde{\alpha}(\boldsymbol{y})} - 1\right)\bar{T}_{,i}(\boldsymbol{x},\boldsymbol{y},p) +$$
$$+ \frac{1}{\eta_0}\frac{\tilde{k}(\boldsymbol{y})}{\tilde{E}(\boldsymbol{y})\tilde{\alpha}(\boldsymbol{y})}\left(\frac{\tilde{E}_{,i}(\boldsymbol{y})}{\tilde{E}(\boldsymbol{y})} + \frac{\tilde{\alpha}_{,i}(\boldsymbol{y})}{\tilde{\alpha}(\boldsymbol{y})}\right)\bar{T}(\boldsymbol{x},\boldsymbol{y},p).$$